Preprints, First IFAC Modeling, Estimation and Control Conference
October 24-27, 2021. Online and UT Austin, USA

Algebraic Car-Following Model Parameter Identification

Zejiang Wang, Xingyu Zhou, and Junmin Wang*
Walker Department of Mechanical Engineering, The University of Texas at Austin
Austin, TX 78712 USA
(e-mail: wangzejiang@utexas.edu, xingyu.zhou@austin.utexas.edu, jwang@austin.utexas.edu)

Abstract: A car-following model describes the longitudinal control strategy of a driver in reaction to the movements of the front cars in the same lane. Because of inter-driver differences, drivers may demonstrate distinct maneuvers in the same excitation of the surrounding traffics. Therefore, the parameters of a car-following model need to be determined per each driver individually. Calibrating a car-following model is commonly treated as a constrained optimization problem. The model parameters, viewed as the optimized variables, are found by minimizing a predefined cost function with a nonlinear numeric solver. However, nonlinear optimization can hardly guarantee global optimality, and more importantly, different formulations of the cost function frequently yield different parameter identification results. To bypass the issues mentioned above, we propose a purely algebraic approach to identify the parameters of a car-following model. Simulation results demonstrate its effectiveness.

Keywords: Algebraic estimation, car-following model, parameter identification.

1. INTRODUCTION

A car-following model describes the longitudinal maneuver of a driver in reaction to the movement of the front vehicles in the same lane. Different car-following models (Chandler *et al*., 1958), (Gazis *et al*., 1959), (Bexelius, 1968), (Tordeux *et al*., 2010) have been proposed since the 1950s, and they are playing an important role in microscopic traffic simulation packages. For instance, car-following models serve as efficient tools to test and evaluate critical components of modern intelligent transportation systems, such as traffic signal control devices (Chen & Sun, 2016) or connected and automated vehicles (Wang *et al*., 2020). Moreover, because of individual differences (Ossen *et al*., 2006, Schnelle *et al*., 2017, Zhang et al., 2017, Schnelle *et al*., 2018), drivers may react to the surrounding traffic in very different ways. With individualized car-following models, we can adapt embedded control algorithms, such as cruise control, to better serve a particular driver (J. Wang *et al*., 2013, Wang & Rajamani, 2004, Ma & Wang, 2021) and powertrain control (Ma & Wang, 2019), and human-centric automated driving (Hu & Wang, 2021).

The discrepancies of drivers' behaviors can be partially reflected in the identified driver model parameters after model calibration. In practice, model calibration is usually treated as a constrained optimization problem: Find $\Theta^* = \min J\left(X - \hat{X}(\Theta)\right)$ such that $\Theta_{lb} \le \Theta \le \Theta_{ub}$. Here, Θ indicates the parameter vector to be determined, and Θ_{lb}, Θ_{ub} are the predefined lower and upper bounds of Θ. X, usually termed as the measure of performance (MOP), is a measured variable and $\hat{X}(\Theta)$ is the simulated counterpart from the car-following model. Finally, J indicates a cost function.

Thus, there exists substantial flexibility for setting up an optimization problem. For instance, X can be selected as ego-car's longitudinal speed, acceleration, inter-vehicle gap distance, time headway, and queue length. Besides, the cost function J can be formulated as squared mean error, mean absolute error, or logged mean absolute error (Hollander & Liu, 2008). Finally, as the explicit mathematical relationship between the cost function and the optimized variables is hard to obtain, a gradient-free numerical solver needs to be selected. However, there exist a large number of candidates, such as genetic algorithm (Kesting & Treiber, 2008), Box's complex method (Balakrishna *et al*., 2007) and downhill simplex method (Tordeux *et al*., 2010).

Unfortunately, as revealed in (Punzo *et al*., 2012), gradient-free solvers are sensitive to the initial optimization point and can frequently lead to local optimality. Consequently, it is not strange to encounter a situation where the identified parameters, which yield a practically low cost function value, are far from true values. Furthermore, different selections of MOP X, along with various formulations of the cost function J can result in distinct parameter identification results. The standardization of setting up the optimization problem is still lacking (Brockfeld *et al*., 2004).

To bypass the difficulties in *numerically* estimating the parameters of a car-following model, we adopt a differential algebra perspective (Diop & Fliess, 1992) to *analytically* identify the parameters of a car-following model. The algebraic method aims at obtaining static and exact formulations of the unknown parameters by performing algebraic operations on the model itself. Consequently, the identification result is independent of the cost function J. Moreover, no numeric solver is required. The key contribution of this paper is to demonstrate the feasibility of applying the algebraic approach for identifying parameters in a car-following model.

The rest of this paper is organized as follows. Section 2 formulates the Bexelius car-following model, which serves as a benchmark to illustrate the proposed algebraic parameter

identification method. Section 3 illustrates, step-by-step, the algebraic parameter identification strategy. Section 4 demonstrates the effectiveness of the proposed method via simulations. Finally, Section 5 concludes this paper.

2. BEXELIUS CAR-FOLLOWING MODEL

The Bexelius model (Bexelius, 1968) is constructed from the CHM car-following model (Chandler et al., 1958) by extending the single-car preview to include the two vehicles ahead of the ego-car. The Bexelius model is graphically presented in Fig. 1.

Fig. 1. Bexelius car-following model.

The Bexelius model reads:

$$\dot{v}_x(t) = c_1 \Delta v_{x1}(t - T_r) + c_2 \Delta v_{x2}(t - T_r). \tag{1}$$

In (1), $\Delta v_{x1}(t) = v_x^{n-1}(t) - v_x(t)$, where $v_x(t)$ is the longitudinal velocity of the ego-car (last car) and $v_x^{n-1}(t)$ represents the longitudinal velocity of the immediate leading car in the same lane. Similarly, $\Delta v_{x2}(t) = v_x^{n-2}(t) - v_x(t)$, with $v_x^{n-2}(t)$ as the longitudinal velocity of the second nearest car in front.

There exist three constants in (1): c_1, c_2 are the sensitivity parameters and T_r is the driver reaction delay. Note that if we only consider the immediate leading car, we have:

$$\dot{v}_x(t) = c_1 \Delta v_{x1}(t - T_r), \tag{2}$$

which is the famous CHM car-following model.

3. ALGEBRAIC PARAMETER IDENTIFICATION

Algebraic parameter identification is rooted in the concept of nonlinear observability: If a parameter can be expressed as a function of system inputs, measurable outputs, as well as their finite order derivatives, then it can be identified (Fliess & Sira–Ramírez, 2003). Unlike Luenberger observer (Luenberger, 1966) or Kalman Filter (Kalman, 1960), algebraic parameter identification is not derived from Lyapunov stability theory. As a consequence, the persistence of excitation condition is not required, and there is no asymptotical convergence phase for the parameter identification.

The workflow to algebraically identify the parameters in (1) is sketched in Fig. 2. The blue and red background colors indicate that the corresponding blocks are executed in the time domain and frequency domain, respectively.

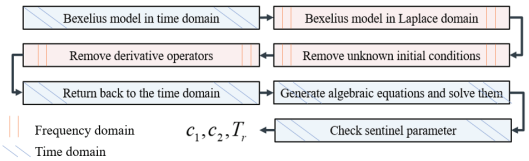

Fig. 2. The workflow of algebraic parameter identification.

Appling Laplace transform on (1) yields:

$$sv_x(s) - v_x(0) = c_1 \Delta v_{x1}(s) e^{-T_r s} + c_2 \Delta v_{x2}(s) e^{-T_r s}. \tag{3}$$

To remove the unknown initial speed condition $v_x(0)$, we differentiate both sides of (3) with respect to the Laplace variable s, and obtain:

$$v_x(s) + s\frac{dv_x(s)}{ds} = \left(c_1 \frac{d\Delta v_{x1}(s)}{ds} - c_1 T_r \Delta v_{x1}(s) + c_2 \frac{d\Delta v_{x2}(s)}{ds} - c_2 T_r \Delta v_{x2}(s)\right) e^{-T_r s}. \tag{4}$$

To continue our analysis, we reformulate the time delay term $e^{-T_r s}$ via the Padé approximation. Since human reaction delay during a car-following process can be as high as 2.2s (Brackstone & McDonald, 1999), we employ the second-degree Padé formula to alleviate the approximation error, as:

$$e^{-T_r s} \approx \frac{12 - 6T_r s + T_r^2 s^2}{12 + 6T_r s + T_r^2 s^2}. \tag{5}$$

The different Padé formulas are compared in Fig. 3, where we use d to indicate the time delay. Hence, using (5) can cogently mitigate the approximation error.

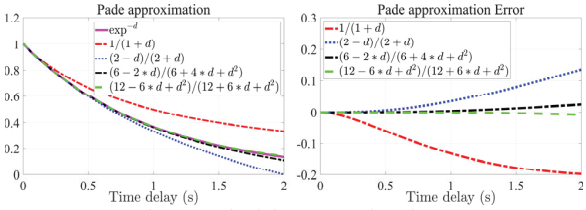

Fig. 3. Padé delay approximation.

Then, we substitute (5) back into (4), and we obtain:

$$v_x(s) + s\frac{dv_x(s)}{ds} = \left(\frac{12 - 6T_r s + T_r^2 s^2}{12 + 6T_r s + T_r^2 s^2}\right) * \left(c_1 \frac{d\Delta v_{x1}(s)}{ds} - c_1 T_r \Delta v_{x1}(s) + c_2 \frac{d\Delta v_{x2}(s)}{ds} - c_2 T_r \Delta v_{x2}(s)\right) \tag{6}$$

Rearranging (6) leads to:

$$\begin{aligned} &12\left(v_x(s) + s\frac{dv_x(s)}{ds}\right) \\ &= -6T_r\left(sv_x(s) + s^2\frac{dv_x(s)}{ds}\right) - T_r^2\left(s^2 v_x(s) + s^3\frac{dv_x(s)}{ds}\right) \\ &+ c_1\left(12\frac{d\Delta v_{x1}(s)}{ds}\right) - c_1 T_r\left(6s\frac{d\Delta v_{x1}(s)}{ds} + 12\Delta v_{x1}(s)\right) \\ &+ c_1 T_r^2\left(s^2\frac{d\Delta v_{x1}(s)}{ds} + 6s\Delta v_{x1}(s)\right) - c_1 T_r^3\left(s^2 \Delta v_{x1}(s)\right) \\ &+ c_2\left(12\frac{d\Delta v_{x2}(s)}{ds}\right) - c_2 T_r\left(6s\frac{d\Delta v_{x2}(s)}{ds} + 12\Delta v_{x2}(s)\right) \\ &+ c_2 T_r^2\left(s^2\frac{d\Delta v_{x2}(s)}{ds} + 6s\Delta v_{x2}(s)\right) - c_2 T_r^3\left(s^2 \Delta v_{x2}(s)\right). \end{aligned} \tag{7}$$

After that, we introduce a sentinel parameter (Garcia-Rodriguez et al., 2009) into (7). Sentinel parameter is an artificial variable to determine when the algebraically identified parameters can be assumed sufficiently close to their true values. Multiplying the left side of (7) with $s+b_x$ and the right side with $s+1$, yields:

$$\begin{aligned}
&12\left(sv_x(s)+s^2\frac{dv_x(s)}{ds}\right)+b_x\left(12v_x(s)+12s\frac{dv_x(s)}{ds}\right)=\\
&-T_r\left(6sv_x(s)+6s^2\left(\frac{dv_x(s)}{ds}+v_x(s)\right)+6s^3\left(\frac{dv_x(s)}{ds}\right)\right)\\
&-T_r^2\left(s^2v_x(s)+s^3\left(\frac{dv_x(s)}{ds}+v_x(s)\right)+s^4\left(\frac{dv_x(s)}{ds}\right)\right)\\
&+c_1\left(12\frac{d\Delta v_{x1}(s)}{ds}+12s\frac{d\Delta v_{x1}(s)}{ds}\right)-c_1T_r^3\left(s^2\Delta v_{x1}(s)+s^3\Delta v_{x1}(s)\right)\\
&-c_1T_r\left(12\Delta v_{x1}(s)+s\left(6\frac{d\Delta v_{x1}(s)}{ds}+12\Delta v_{x1}(s)\right)+s^2\left(6\frac{d\Delta v_{x1}(s)}{ds}\right)\right)\\
&+c_1T_r^2\left(6s\Delta v_{x1}(s)+s^2\left(\frac{d\Delta v_{x1}(s)}{ds}+6\Delta v_{x1}(s)\right)+s^3\left(\frac{d\Delta v_{x1}(s)}{ds}\right)\right)\\
&+c_2\left(12\frac{d\Delta v_{x2}(s)}{ds}+12s\frac{d\Delta v_{x2}(s)}{ds}\right)-c_2T_r^3\left(s^2\Delta v_{x2}(s)+s^3\Delta v_{x2}(s)\right)\\
&-c_2T_r\left(12\Delta v_{x2}(s)+s\left(6\frac{d\Delta v_{x2}(s)}{ds}+12\Delta v_{x2}(s)\right)+s^2\left(6\frac{d\Delta v_{x2}(s)}{ds}\right)\right)\\
&+c_2T_r^2\left(6s\Delta v_{x2}(s)+s^2\left(\frac{d\Delta v_{x2}(s)}{ds}+6\Delta v_{x2}(s)\right)+s^3\left(\frac{d\Delta v_{x2}(s)}{ds}\right)\right).
\end{aligned}\tag{8}$$

As will be shown later, by observing the value of the sentinel parameter b_x we can deduce the convergence status of the other estimated parameters.

Before converting (8) back into the time domain, we first multiply s^{-5} on both sides of (8) and move all the unknown parameters to the right side, as:

$$\begin{aligned}
&12\left(s^{-4}v_x(s)+s^{-3}\frac{dv_x(s)}{ds}\right)=-b_x\left(s^{-5}\left(12v_x(s)\right)+s^{-4}\left(12\frac{dv_x(s)}{ds}\right)\right)\\
&-T_r\left(s^{-4}\left(6v_x(s)\right)+s^{-3}\left(6\frac{dv_x(s)}{ds}+6v_x(s)\right)+s^{-2}\left(6\frac{dv_x(s)}{ds}\right)\right)\\
&-T_r^2\left(s^{-3}v_x(s)+s^{-2}\left(\frac{dv_x(s)}{ds}+v_x(s)\right)+s^{-1}\left(\frac{dv_x(s)}{ds}\right)\right)\\
&+c_1\left(s^{-5}\left(12\frac{d\Delta v_{x1}(s)}{ds}\right)+s^{-4}\left(12\frac{d\Delta v_{x1}(s)}{ds}\right)\right)-c_1T_r^3\left(s^{-3}\Delta v_{x1}(s)+s^{-2}\Delta v_{x1}(s)\right)\\
&-c_1T_r\left(s^{-5}\left(12\Delta v_{x1}(s)\right)+s^{-4}\left(6\frac{d\Delta v_{x1}(s)}{ds}+12\Delta v_{x1}(s)\right)+s^{-3}\left(6\frac{d\Delta v_{x1}(s)}{ds}\right)\right)\\
&+c_1T_r^2\left(s^{-4}\left(6\Delta v_{x1}(s)\right)+s^{-3}\left(\frac{d\Delta v_{x1}(s)}{ds}+6\Delta v_{x1}(s)\right)+s^{-2}\left(\frac{d\Delta v_{x1}(s)}{ds}\right)\right)\\
&+c_2\left(s^{-5}\left(12\frac{d\Delta v_{x2}(s)}{ds}\right)+s^{-4}\left(12\frac{d\Delta v_{x2}(s)}{ds}\right)\right)-c_2T_r^3\left(s^{-3}\Delta v_{x2}(s)+s^{-2}\Delta v_{x2}(s)\right)\\
&-c_2T_r\left(s^{-5}\left(12\Delta v_{x2}(s)\right)+s^{-4}\left(6\frac{d\Delta v_{x2}(s)}{ds}+12\Delta v_{x2}(s)\right)+s^{-3}\left(6\frac{d\Delta v_{x2}(s)}{ds}\right)\right)\\
&+c_2T_r^2\left(s^{-4}\left(6\Delta v_{x2}(s)\right)+s^{-3}\left(\frac{d\Delta v_{x2}(s)}{ds}+6\Delta v_{x2}(s)\right)+s^{-2}\left(\frac{d\Delta v_{x2}(s)}{ds}\right)\right).
\end{aligned}\tag{9}$$

Therefore, no derivative operations $s^\alpha, \alpha\in \mathrm{N}^+$ will appear in the time domain when we convert (9) back to the time domain. In this case, high-frequency measurement noises will not be amplified. Moreover, all the measured variables, i.e., $v_x(t)$, $\Delta v_{x1}(t)$, and $\Delta v_{x2}(t)$ in (9), will be integrated at least once. The integration serves as a low-pass filter to wipe out high-frequency measurement noises.

Recall that the inverse Laplace transform reads:

$$\begin{cases}
\mathcal{L}^{-1}\{s(\bullet)\}=d(\bullet)/dt,\\
\mathcal{L}^{-1}\{d^v(\bullet)/ds^v\}=(-t)^v(\bullet),\\
\mathcal{L}^{-1}\{(\bullet)/s\}=\int_0^t(\bullet)(\tau)\,d\tau.
\end{cases}\tag{10}$$

Applying (10) on (9) yields a linearly identifiable form, in terms of the unknown parameter set, as:

$$P_{Bex}(t)^T\,\Theta_{Bex}=q_{Bex}(t),\tag{11}$$

with $\Theta_{Bex}=\left[-b_x,-T_r,-T_r^2,c_1,-c_1T_r,c_1T_r^2,-c_1T_r^3,c_2,-c_2T_r,c_2T_r^2,-c_2T_r^3\right]$, and $P_{Bex}(t)=\left[p_1(t),p_2(t),\ldots,p_{10}(t),p_{11}(t)\right]^T$, where

$$p_1(t)=12\left(\int^5 v_x(t)+\int^4 -tv_x(t)\right),\tag{12}$$

$$p_2(t)=6\left(\int^4 v_x(t)+\int^3 -tv_x(t)+v_x(t)+\int^2 -tv_x(t)\right),\tag{13}$$

$$p_3(t)=\int^3 v_x(t)+\int^2 -tv_x(t)+v_x(t)-\int tv_x(t),\tag{14}$$

$$p_4(t)=12\left(\int^5 -t\Delta v_{x1}(t)+\int^4 -t\Delta v_{x1}(t)\right),\tag{15}$$

$$p_5(t)=12\int^5\Delta v_{x1}(t)+\int^4 -6t\Delta v_{x1}(t)+12\Delta v_{x1}(t)+\int^3 -6t\Delta v_{x1}(t),\tag{16}$$

$$p_6(t)=6\int^4\Delta v_{x1}(t)+\int^3 6\Delta v_{x1}(t)-t\Delta v_{x1}(t)+\int^2 -t\Delta v_{x1}(t),\tag{17}$$

$$p_7(t)=\int^3\Delta v_{x1}(t)+\int^2\Delta v_{x1}(t),\tag{18}$$

$$p_8(t)=12\left(\int^5 -t\Delta v_{x2}(t)+\int^4 -t\Delta v_{x2}(t)\right),\tag{19}$$

$$p_9(t)=12\int^5\Delta v_{x2}(t)+\int^4 -6t\Delta v_{x2}(t)+12\Delta v_{x2}(t)+\int^3 -6t\Delta v_{x2}(t),\tag{20}$$

$$p_{10}(t)=6\int^4\Delta v_{x2}(t)+\int^3 6\Delta v_{x2}(t)-t\Delta v_{x2}(t)+\int^2 -t\Delta v_{x2}(t),\tag{21}$$

$$p_{11}(t)=\int^3\Delta v_{x2}(t)+\int^2\Delta v_{x2}(t),\tag{22}$$

and

$$q_{Bex}(t)=12\left(\int^{4}v_x(t)+\int^{3}-tv_x(t)\right). \tag{23}$$

Note that we use $\int^{(n)}\phi(t)$ to represent the iterated integrals $\int_{t_0}^{t}\int_{t_0}^{\sigma_1}\cdots\int_{t_0}^{\sigma_{n-1}}\phi(\sigma_n)d\sigma_n\cdots d\sigma_1$, with $t_0=0$. Especially, if $n=1$, we simplify $\int^{(1)}\phi(t)$ as $\int\phi(t)$.

Note that there are eleven unknown parameters in (11). In other words, we have an underdetermined equation. The common method to solve this underdetermined equation is to formulate a least-squares problem, as:

$$\Theta_{Bex}^{*}=\arg\min_{\Theta_{Bex}}J(\Theta_{Bex},t), \tag{24}$$

where

$$J(\Theta_{Bex},t)=\int_0^t\left(P_{Bex}(\tau)^T\Theta_{Bex}-q_{Bex}(\tau)\right)^2d\tau. \tag{25}$$

Assigning

$$M_{Pq}=\int_0^t P_{Bex}(\tau)q_{Bex}(\tau)d\tau, \tag{26}$$

$$M_{PP}=\int_0^t P_{Bex}(\tau)P_{Bex}^T(\tau)d\tau, \tag{27}$$

$$M_{qP}=M_{Pq}{}^T=\int_0^t q_{Bex}(\tau)P_{Bex}^T(\tau)d\tau, \tag{28}$$

$$M_{qq}=\int_0^t q_{Bex}(\tau)q_{Bex}(\tau)d\tau, \tag{29}$$

we can reformulate (25) as:

$$\begin{aligned}J(\Theta_{Bex},t)&=M_{qq}-M_{qP}\Theta_{Bex}-\Theta_{Bex}^TM_{Pq}+\Theta_{Bex}^TM_{PP}\Theta_{Bex}\\&=\left(\Theta_{Bex}-(M_{PP})^{-1}M_{Pq}\right)^TM_{PP}\left(\Theta_{Bex}-(M_{PP})^{-1}M_{Pq}\right)\\&\quad+M_{qq}-M_{qP}(M_{PP})^{-1}M_{Pq}.\end{aligned} \tag{30}$$

Therefore, the optimal Θ_{Bex} to minimize (25) can be *analytically* derived as:

$$\Theta_{Bex}^{*}=(M_{PP})^{-1}M_{Pq}, \tag{31}$$

where

$$M_{PP}=\int_0^t P_{Bex}(\tau)P_{Bex}^T(\tau)d\tau=\begin{bmatrix}\int_0^t p_1(\tau)p_1(\tau)d\tau & \int_0^t p_1(\tau)p_2(\tau)d\tau & \cdots & \int_0^t p_1(\tau)p_{11}(\tau)d\tau\\ \int_0^t p_2(\tau)p_1(\tau)d\tau & \ddots & & \vdots\\ \vdots & & \ddots & \vdots\\ \int_0^t p_{11}(\tau)p_1(\tau)d\tau & \cdots & \cdots & \int_0^t p_{11}(\tau)p_{11}(\tau)d\tau\end{bmatrix}, \tag{32}$$

$$M_{Pq}=\int_0^t P_{Bex}(\tau)q_{Bex}(\tau)d\tau=\left[\int_0^t p_1(\tau)q_{Bex}(\tau)d\tau,\int_0^t p_2(\tau)q_{Bex}(\tau)d\tau,\ldots,\int_0^t p_{11}(\tau)q_{Bex}(\tau)d\tau\right]^T. \tag{33}$$

Note that at $t=0$, (31) is indefinite as matrix M_{PP} is singular. However, since M_{PP} is positive semi-definite, its numeric condition shall improve as time goes by. Once the minimum absolute eigenvalue of M_{PP} becomes far away from zero, (31) yields the reliably identified parameters.

4. SIMULATION RESULTS

In this section, we utilize Matlab simulation to verify the proposed algebraic parameter identifier. As shown in Fig. 1, speed profiles of a three-car-platoon are required. In this paper, $v_x^{n-1}(t)$ and $v_x^{n-2}(t)$ are retrieved from the reconstructed NGSIM dataset (Coifman & Li, 2017). Meanwhile, the synthetic speed profile $v_x(t)$ of the last car is generated from the Bexelius model (1) with predefined parameters $c_1^{*}=0.8$, $c_2^{*}=0.3$, and $T_r^{*}=0.5$. Profiles of $v_x^{n-1}(t)$, $v_x^{n-2}(t)$, and $v_x(t)$ are exhibited in Fig. 4.

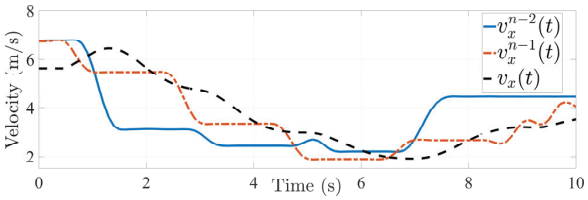

Fig. 4. Three car speed profiles.

Note that the dataset in (Coifman & Li, 2017) is retrieved from a video record of the I-80 highway near San Francesco, from 4:00 PM to 4:15 PM. Therefore, typical speed profiles in a congested traffic scenario are demonstrated in Fig. 4.

As we mentioned in Section 3, algebraic identification does not maintain an asymptotical convergence phase. Instead, the convergence of the identification is determined by the numeric condition of the matrix M_{PP}. To determine when the estimated parameters from (31) can be assumed close to their true values, we leverage the estimated sentinel parameter $\hat{b}_x$. Unlike the other unknown parameters, the ground truth value of the sentinel parameter, $b_x=1$, is known *a priori* in (8). As $\hat{b}_x$ is estimated similar to all the rest parameters, we can reasonably conjecture that when $\hat{b}_x$ remains close to 1, the estimated $\hat{T}_r$, $\hat{c}_1$, and $\hat{c}_2$, shall also be near their corresponding actual values (Garcia-Rodriguez et al., 2009). Precisely speaking, $\hat{T}_r=-\Theta_{Bex}^{*}(2)$, $\hat{c}_1=\Theta_{Bex}^{*}(4)$, and $\hat{c}_2=\Theta_{Bex}^{*}(8)$ (see (11)) are outputted as the estimated parameters when the following two criteria are met:

$$\begin{cases}\left|\sigma(\hat{b}_x)\big/E(\hat{b}_x)\right|\le\Delta_{\text{var}},\\ \left|\hat{b}_x-1\right|\le\Delta_{cls}.\end{cases} \tag{34}$$

In (34), $E(\hat{b}_x)=\int_{t-T_{win}}^{t}\hat{b}_x(\tau)d\tau\big/T_{win}$ is the moving-averaged identified sentinel parameter $\hat{b}_x$, with T_{win} as the sliding

window length. $\sigma\left(\hat{b}_x\right)=\sqrt{E\left[\hat{b}_x{}^2\right]-\left(E\left[\hat{b}_x\right]\right)^2}$ represents the variance of $\hat{b}_x$. Finally, Δ_{var} and Δ_{cls} are the thresholds. The first criterion in (34) ensures that the estimated sentinel parameter enters into its steady-state, and the second criterion guarantees its estimation correctness. Intuitively, the selection of Δ_{var} and Δ_{cls} trades off between the estimation accuracy and speed. A smaller threshold value could yield a more accurate estimation result with the cost of a longer convergence period.

Once (34) is met, we can permanently stop the estimation and output the estimated variables if we know the parameters are strictly constant. On the contrary, if the identified parameters are slowly time-varying, we can approximate them as piece-wise constant parameters and periodically reset (33) to obtain refreshed parameters (Linares-Flores et al., 2014). In the following, we fix $\Delta_{\text{var}}=1e-5$ and $\Delta_{cls}=1e-2$.

We first demonstrate the estimation of the sentinel parameter b_x in Fig. 5.

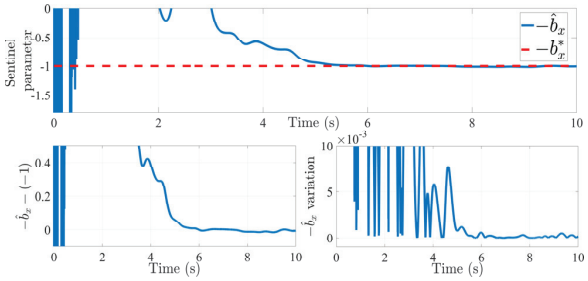

Fig. 5. Estimation of the minus sentinel parameter.

The upper subplot in Fig. 5 comes from $\Theta_{Bex}^*(1)$, which corresponds to $-\hat{b}_x$. At the beginning of the estimation, because of the singularity of M_{PP} in (31), the estimated sentinel parameter demonstrates strong oscillations, which is well captured by $\left|\sigma\left(\hat{b}_x\right)/E\left(\hat{b}_x\right)\right|$ in (34). As the condition number of M_{PP} decreases, the estimated sentinel parameter gradually converges and remains close to its true value: $-\hat{b}_x\to -1$. At around $t\approx 5.7s$, criteria (34) become satisfied, and we obtain $\hat{T}_r$, $\hat{c}_1$, and $\hat{c}_2$.

The estimated $\Theta_{Bex}^*(2)$, $\Theta_{Bex}^*(4)$ and $\Theta_{Bex}^*(8)$ are compiled in Fig. 6.

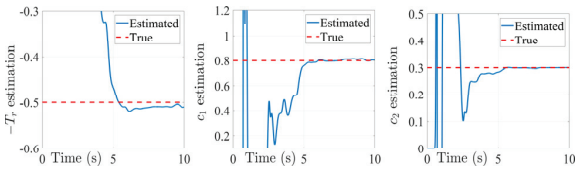

Fig. 6. Identification of parameters of interest.

Similar to the sentinel parameters, the estimated $-\hat{T}_r$, $\hat{c}_1$, and $\hat{c}_2$ exhibit strong oscillations at the beginning of the identification process and gradually, but not asymptotically, converge into their corresponding true values. At $t\approx 5.7s$, the finally outputted identification results are summarized in Table 1.

Table 1. Final parameter identification results.

	$-T_r$	c_1	c_2
Identification result	-0.5097	0.7868	0.3009
True value	-0.5000	0.8000	0.3000
Estimation error	1.94%	1.65%	0.30%

Therefore, the algebraic approach yields quite accurate parameter identification results. As indicated in Fig. 4, the excitation level of the system inputs $\left(\Delta v_{x1}(t),\Delta v_{x2}(t)\right)$ is quite limited in a congested traffic scenario. Therefore, we need to wait a long enough period until M_{PP} in (33) becomes somehow well-conditioned. This fact partially explains the parameter estimation errors and the relatively slower identification process.

Remark 1: Before criteria (34) become satisfied, no trustful parameter identification results from (33) can be available. In this case, we can rely on the offline identified parameters from the historical driving data of a specific driver.

Remark 2: Comparison between the algebraic approach and the typical recursive least squares (RLS) method for parameter identification can be found in the authors' previous paper (Zejiang Wang & Wang, 2020).

5. CONCLUSIONS

In this paper, we propose an algebraic parameter identification approach for the Bexelius car-following model. In contrast to the traditional optimization-based model calibration approach, no explicit cost function needs to be designed *a priori*, and no numerical optimization process is involved. Simulation results demonstrate the effectiveness of the proposed strategy. Indeed, the algebraic parameter identification framework can be applied to a class of car-following models, which can be expressed as its linear identifiable form in terms of the unknown parameters, akin to (11). Typical examples include the CHM model (Chandler et al., 1958), the GHR model (Gazis et al., 1959), and the adaptive gap-time model (Tordeux et al., 2010). We will study using the algebraic approach to identify time-varying parameters under the influence of modeling errors.

ACKNOWLEDGEMENT

The authors would like to thank the financial support partially provided by NSF with award number 1901632.

REFERENCES

Balakrishna, R., Antoniou, C., Ben-Akiva, M., Koutsopoulos, H. N., and Wen, Y. (2007). Calibration of Microscopic Traffic Simulation Models. Transportation Research Record: Journal of the Transportation Research Board,

1999(1), 198–207.
Bexelius, S. (1968). An extended model for car-following. Transportation Research, 2(1), 13–21.
Brackstone, M., and McDonald, M. (1999). Car-following: A historical review. In Transportation Research Part F: Traffic Psychology and Behaviour (Vol. 2, Issue 4, pp. 181–196). Elsevier Ltd.
Brockfeld, E., Kühne, R. D., and Wagner, P. (2004). Calibration and Validation of Microscopic Traffic Flow Models. Transportation Research Record: Journal of the Transportation Research Board, 1876(1), 62–70.
Chandler, R. E., Herman, R., and Montroll, E. W. (1958). Traffic Dynamics: Studies in Car Following. Operations Research, 6(2), 165–184.
Chen, S., and Sun, D. J. (2016). An Improved Adaptive Signal Control Method for Isolated Signalized Intersection Based on Dynamic Programming. IEEE Intelligent Transportation Systems Magazine, 8(4), 4–14.
Coifman, B., and Li, L. (2017). A critical evaluation of the Next Generation Simulation (NGSIM) vehicle trajectory dataset. Transportation Research Part B: Methodological, 105, 362–377.
Diop, S., and Fliess, M. (1992). Nonlinear observability, identifiability, and persistent trajectories. Proceedings of the IEEE Conference on Decision and Control, 714–719.
Fliess, M., and Sira–Ramírez, H. (2003). An algebraic framework for linear identification. ESAIM: Control, Optimisation and Calculus of Variations, 9, 151–168.
Garcia-Rodriguez, C., Cortes-Romero, J. A., and Sira-Ramirez, H. (2009). Algebraic identification and discontinuous control for trajectory tracking in a perturbed 1-DOF suspension system. IEEE Transactions on Industrial Electronics, 56(9), 3665–3674.
Gazis, D. C., Herman, R., and Potts, R. B. (1959). Car-Following Theory of Steady-State Traffic Flow. Operations Research, 7(4), 499–505.
Hollander, Y., and Liu, R. (2008). The principles of calibrating traffic microsimulation models. Transportation, 35(3), 347–362.
Hu, C. & Wang, J. (2021). Trust-Based and Individualizable Adaptive Cruise Control Using Control Barrier Function Approach with Prescribed Performance. IEEE Transactions on Intelligent Transportation Systems (in press).
Kalman, R. E. (1960). A new approach to linear filtering and prediction problems. Journal of Fluids Engineering, Transactions of the ASME, 82(1), 35–45.
Kesting, A., and Treiber, M. (2008). Calibrating Car-Following Models by Using Trajectory Data. Transportation Research Record: Journal of the Transportation Research Board, 2088(1), 148–156.
Linares-Flores, J., Hernandez Mendez, A., Garcia-Rodriguez, C., and Sira-Ramirez, H. (2014). Robust nonlinear adaptive control of a “boost” converter via algebraic parameter identification. IEEE Transactions on Industrial Electronics, 61(8), 4105–4114.
Luenberger, D. G. (1966). Observers for Multivariable Systems. IEEE Transactions on Automatic Control, 11(2), 190–197.
Ma, Yao and Wang, Junmin. (2021). Energetic Impacts Evaluation of Eco-Driving on Mixed Traffic with Driver Behavioral Diversity. IEEE Transactions on Intelligent Transportation Systems (in press).
Ma, Yao and Wang, Junmin. (2019). Predictive Control for NOx Emission Reductions in Diesel Engine Vehicle Platoon Application. IEEE Transactions on Vehicular Technology. 68(7), 6429 – 6440, 2019.
Ossen, S., Hoogendoorn, S. P., and Gorte, B. G. H. (2006). Interdriver Differences in Car-Following. Transportation Research Record: Journal of the Transportation Research Board, 1965(1), 121–129.
Punzo, V., Ciuffo, B., and Montanino, M. (2012). Can Results of car-following Model Calibration Based on Trajectory Data be Trusted? Transportation Research Record: Journal of the Transportation Research Board, 2315(1), 11–24.
Schnelle, S., Wang, J., Su, H., and Jagacinski, R. (2017). A Personalizable Driver Steering Model Capable of Predicting Driver Behaviors in Vehicle Collision Avoidance Maneuvers. IEEE Transactions on Human-Machine Systems, Vol. 47, Issue 5, pp. 625 – 635.
Schnelle, S., Wang, J., Jagacinski, R., and Su, H. (2018). A Feedforward and Feedback Integrated Lateral and Longitudinal Driver Model for Personalized Advanced Driver Assistance Systems. Mechatronics, Vol. 50, pp. 177 – 188.
Tordeux, A., Lassarre, S., and Roussignol, M. (2010). An adaptive time gap car-following model. Transportation Research Part B: Methodological, 44(8–9), 1115–1131.
Wang, J. and Rajamani, R. (2004). The Impact of Adaptive Cruise Control Systems on Highway Safety and Traffic Flow. Journal of Automobile Engineering, Proceedings of the Institution of Mechanical Engineers, Part D, 218 (2), 111 – 130.
Wang, J., Zhang, L., Zhang, D., and Li, K. (2013). An adaptive longitudinal driving assistance system based on driver characteristics. IEEE Transactions on Intelligent Transportation Systems, 14(1), 1–12.
Wang, Z., and Wang, J. (2020). Real-time driver model parameter identification: An algebraic approach. ASME 2020 Dynamic Systems and Control Conference.
Wang, Ziran, Wu, G., and Barth, M. J. (2020). Cooperative Eco-Driving at Signalized Intersections in a Partially Connected and Automated Vehicle Environment. IEEE Transactions on Intelligent Transportation Systems, 21(5), 2029–2038.
Zhang, S., Luo, Y., Wang, J., Wang, X., and Li, K. 2017. Predictive Energy Management Strategy for Fully Electric Vehicles based on Preceding Vehicle Movement. IEEE Transactions on Intelligent Transportation Systems, Vol. 18, Issue 11, pp. 3049 – 3060.